Materials and Design 191 (2020) 108613

Contents lists available at ScienceDirect

Materials and Design

journal homepage: www.elsevier.com/locate/matdes

Effects of Cr addition on the constitutive equation and precipitated phases of copper alloy during hot deformation

Yijie Ban [a,b,c], Yi Zhang [a,b,c,*], Yanlin Jia [d,e,**], Baohong Tian [a,b,c], Alex A. Volinsky [f], Xiaohui Zhang [a,b,c], Qifei Zhang [a,b,c], Yongfeng Geng [a,b,c], Yong Liu [a,b,c], Xu Li [g]

[a] School of Materials Science and Engineering, Henan University of Science and Technology, Luoyang 471023, PR China
[b] Collaborative Innovation Center of Nonferrous Metals, Henan Province, Luoyang 471023, PR China
[c] Henan Key Laboratory of Nonferrous Materials Science and Processing Technology, Luoyang 471023, PR China
[d] College of Materials Science and Engineering, Beijing University of Technology, Beijing 100124, PR China
[e] School of Materials Science and Engineering, Central South University, Changsha 410083, China
[f] Department of Mechanical Engineering, University of South Florida, Tampa 33620, USA
[g] Center for Advanced Measurement Science, National Institute of Metrology, Beijing 100029, PR China

HIGHLIGHTS

- The addition of Cr can obtain more precipitates.
- The addition of Cr can inhibit the dynamic recrystallization of Cu-Ni-Co-Si alloy.
- The size of precipitated phase decreases obviously with the addition of Cr elements.

GRAPHICAL ABSTRACT

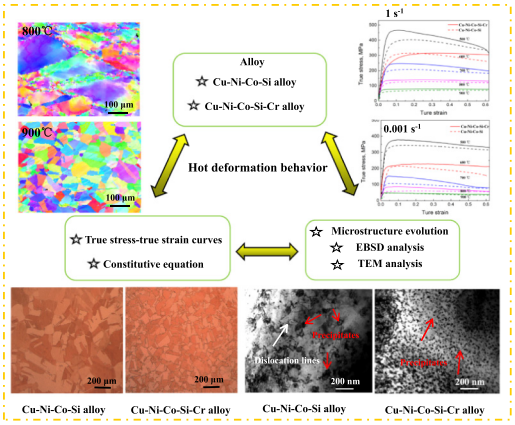

ARTICLE INFO

Article history:
Received 11 November 2019
Received in revised form 3 February 2020
Accepted 27 February 2020
Available online 05 March 2020

Keywords:
Cu-Ni-Co-Si-Cr alloy
Hot deformation
Constitutive equations
Texture change
Precipitated phase

ABSTRACT

The Cu-Ni-Si alloy has widely applications in the lead frames and electronics industries due to its high strength and conductivity. In this work, hot deformation behavior of the Cu-1.5Ni-1.1Co-0.6Si and Cu-1.5Ni-1.1Co-0.6Si-0.1Cr alloys were investigated through the isothermal compression tests using the Gleeble-1500D thermo-mechanical simulator operating at the temperature ranging from 500 °C to 900 °C and 0.001–10 s^{-1} strain rate. The deformed microstructure was characterized by the electron backscatter diffraction (EBSD) and the transmission electron microscopy. The constitutive equations of the alloys were established. According to the microstructure analysis, it can be observed that the grain size of the alloy with Cr was more uniform. In addition, the misorientation angle of 14.19 during recrystallization was significantly lower than 24 after the recrystallization, which means that the migration rate of grain boundaries is slow. The texture of the Cu-Ni-Co-Si alloy at 800 °C is the Goss {011}⟨100⟩ texture and {001}⟨100⟩ cubic texture, while the Goss texture at 900 °C is replaced by the {011} ⟨112⟩brass texture. The effects of Cr on precipitation phases were analyzed, and the precipitated

* Correspondence to: Y. Zhang, School of Materials Science and Engineering, Henan University of Science and Technology, Luoyang 471023, PR China.
** Corresponding author.
E-mail addresses: yizhang@haust.edu.cn (Y. Zhang), jiayanlin@bjut.edu.cn (Y. Jia).

https://doi.org/10.1016/j.matdes.2020.108613

phases were $(Ni, Co)_2Si$, Co_2Si. The addition of Cr promoted precipitation and significantly reduced the precipitate size. The addition of Cr can improve the strength and activation energy of the alloy. The activation energy was 569.8 kJ/mol and 639.5 kJ/mol, respectively.

1. Introduction

Copper alloys are widely used in the lead frames and electronic devices due to their improved properties [1–3]. These alloys include Cu-Be [4], Cu-Cr [5], Cu-Ti [6], Cu-Sn [7], and Cu-Ni-Si [8]. However, toxicity and stress relaxation of Be affect processing and industrial applications. Cu-Cr, Cu-Ti, and Cu-Sn have high strength, but much lower electrical conductivity than the Cu-Be alloy. The Cu-Ni-Si alloy not only has good strength but adequate electrical conductivity. With the Ni and Si content is low, the strength and conductivity of the Cu-Ni-Si alloy can reach 800 MPa and 45% IACS (International Annealed Copper Standard), respectively. With the Ni and Si content is high, the strength can reach over 1000 MPa, which is good for application prospects [9,10].

Hot deformation is the fundamental part of thermal processing, and widely applied in manufacture industry to improve the properties of alloys. The temperature, strain rate and microstructure evolution during hot deformation are important to optimize the hot deformation process, and finally affect the properties of the products. According to the above mentioned, the simulation of the hot deformation process can obtain the optimal deformation parameters to avoid macro cracks and non-homogeneous microstructure in products. The precipitations occur during the hot deformation which was defined as dynamic precipitation including discontinuous phase transformation and dynamic coarsening precipitates has a great affected on hardness and strength of the alloys. Dynamic precipitation is notably accelerated by deformation and proceeds faster than the static aging. In the hot deformation test of Cu-Ni-Si-Cr-Mg alloy investigated by L. Blaz et al. [11,12] found that after the solid solution treatment of the sample could effective improve the dynamic precipitation. Dynamic precipitation can effectively enhance the work hardening of the alloy, especially at medium temperature (673–773k). At high temperature leads to the coarsening of Ni_2Si particles, reduction of the material hardness and strength. It is worth noting that the coarsening of the precipitated phase at the sheared areas are faster than that in the grain interiors, which is responsible for the flow localization and softening.

Previous studies of Cu-Ni-Si mainly focused on aging precipitation behaviors, but only a few studies focused on the hot deformation behaviors. In this paper, the thermal deformation of the Cu-Ni-Si alloy was studied by the addition of Co and Cr. The addition of Co is widely used in semiconductor devices. The addition of Co can improve the formation of the Co_2Si precipitates [13]. Krishna et al. found that δ-Ni_2Si can increase the hardness of the alloy, and a small amounts of Co can replace Ni to form $(Ni, Co)_2Si$ precipitates, which greatly improve the strength and hardness [14,15]. Furthermore, some researchers reported that Cr can improve the mechanical properties of the alloy, while it has little effect on the alloy electrical conductivity. The addition of Cr can significantly refine the structure, which is very beneficial to the productions through the conventional melting and casting method. The addition of Cr can play an obviously role in improving the stability at high temperatures. Specifically, nano-precipitated Cr can inhibit the grain growth and improve mechanical properties of the alloy [16–19]. In addition, the Cr element has much less effect on the conductivity of the alloy compared with some other elements, which is due to very low solubility of Cr in the copper matrix and the precipitation related with Cr. Besides, the Cr particles can precipitate from the copper matrix during aging at medium temperature, which improve the electrical property of alloy. In this paper, the addition of Cr element is expected to develop new copper alloys with high mechanical and electrical properties.

In this work, hot deformation behaviors of the Cu-1.5Ni-1.1Co-0.6Si and Cu-1.5Ni-1.1Co-0.6Si-0.1Cr alloys were studied according to the isothermal compression testing, which was conducted on the Geeble-1500D thermo-mechanical simulator. The microstructure evolutions and flow stress behaviors were studied at the deformation temperature ranges of 500–900 °C and strain rates of 0.001–10 s^{-1}. The constitutive equations of Cu-1.5Ni-1.1Co-0.6Si and Cu-1.5Ni-1.1Co-0.6Si-0.1Cr alloys were established, respectively. In order to analyze the microstructure and orientation of alloys under various processing conditions, the EBSD (electron backscatter diffraction) was used to observe the texture of recrystallization period and recrystallization completion period, respectively. In order to clarify the effects of Cr addition on precipitates of Cu-1.5Ni-1.1Co-0.6Si and Cu-1.5Ni-1.1Co-0.6Si-0.1Cr alloys during hot deformation, the structure evolutions of the two alloys were analyzed by TEM deformed at 800 °C and 0.001 s^{-1}.

2. Experimental procedures

The chemical composition of the Cu-Ni-Co-Si and Cu-Ni-Co-Si-Cr alloy is listed in Table 1. The 99.95 wt% standard cathode copper, Ni, Co, Si, Cr master alloy was prepared and melted in the ZG-0.01 vacuum medium frequency induction furnace under argon atmosphere to prevent oxidation. The ingots were heated to 1000 °C for 2 h and then extruded into Ø 35 mm diameter bars using the XJ-500 metal profile extrusion machine, followed by air cooling. The samples were solution treated at 950 °C for 2 h by using the KSS-1200 tubular resistance furnace and then water quenched. The samples were machined into Ø 8 mm × 12 mm cylinders for hot compression testing. The samples were compressed using the Gleeble-1500D thermo-mechanical simulator. The range of the deformation temperature was 500–900 °C and the range of the strain rates was 0.001 s^{-1}–10 s^{-1}. The samples were heated to the target temperature at the rate of 10 °C/s and kept at that temperature for 3 min before undergoing 55% compression. Argon atmosphere was introduced during compression to prevent oxidation. The samples were quenched in water for <2 s to maintain the high-temperature microstructure.

The cutting direction of the samples was parallel to the direction of deformation. The schematic illustration of the complete test and the sample state is shown in Fig. 1. The samples were cut and the center part was used for polishing. The specimens were etched in the 5 g $FeCl_3$, 10 mL HCl, and 100 mL distilled water solution. The OLYMPUS PMG3 optical microscope was used in microstructure observation. The EBSD images were observed by using a JMS-7800F field emission scanning electron microscope (SEM) with a step size of 0.5 um and a voltage of 20 KV. The software Transmission Channel 5 was used to analyze the EBSD data. The specimens were electropolished in a solution containing 50% alcohol and 50% phosphoric acid at 20 °C and a voltage of 5 V. The TEM and HRTEM images were obtained by using the JEM-2100F transmission electron microscope with a voltage of 200 kV and 0.19 nm resolution. The specimen was processed into a wafer with a thickness

Table 1
Chemical composition of the designed alloy (mass fraction, %).

Alloy	Si	Ni	Co	Cr	Cu
Cu-Ni-Co-Si	0.6	1.5	1.1	–	bal.
Cu-Ni-Co-Si-Cr	0.6	1.5	1.1	0.1	bal.

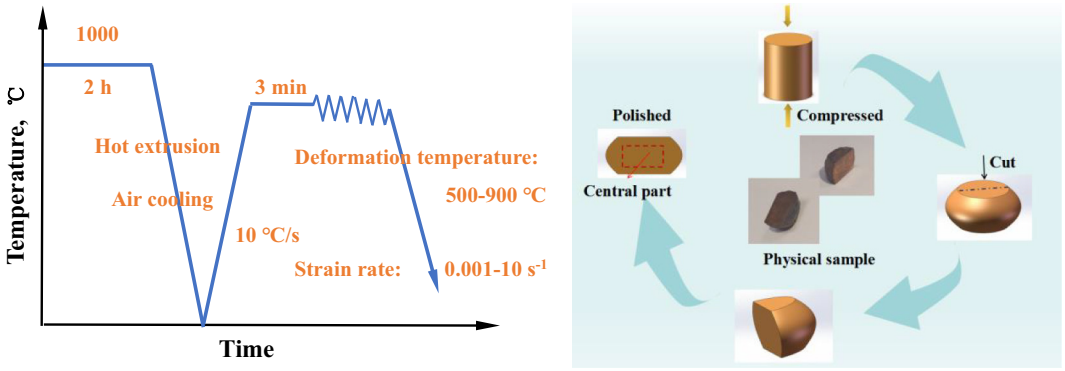

Fig. 1. Schematic illustration of the complete test and sample state.

of 50 um and a diameter of 3 mm, and subsequently ion thinned using Gatan 691 ion beam thinner.

3. Results

Fig. 2 demonstrates the solid solution microstructure of the Cu-Ni-Co-Si and Cu-Ni-Co-Si-Cr alloys. The grain size of the Cu-Ni-Co-Si-Cr alloy is low with respect to the Cu-Ni-Co-Si alloy. This indicates that Cr addition can refine grains. Furthermore, grain refinement can improve mechanical properties, such as strength and toughness. In other words, when the grain size is small and the grain boundary area is large, it can effectively prevent dislocation movement and slip between grains, making the material less prone to fracture [20].

3.1. True stress–true strain curves

Fig. 3 shows the true stress-true strain curves of the Cu-Ni-Co-Si and Cu-Ni-Co-Si-Cr alloys at different temperatures and strain rates. (In order to ensure the accuracy of the data, repeated experiments were conducted. The data in the figure is the average value.) During the hot deformation process, the true stress-true strain curve changes are mainly from the changes in superposition of strain hardening, precipitation hardening, dynamic recovery and dynamic recrystallization (DRX), respectively. At the low-temperature zone (500–700 °C), the flow stress increases rapidly to the peak value. The work hardening is the main mechanism at this stage. Work hardening is attributed to the grain slippage of the alloy at low temperature and high strain rate. The slip surface and the lattice are distorted, and dislocations are entangled at this time with strong interactions. Thus, dislocation movement is inhibited resulting in the flow stress increase. In this stage, precipitation hardening plays a significant role in enhancing the stress value. The fine dynamic precipitation occurs can increase the hardness of the alloy. With the increase of strain degrees, the dynamic precipitation is coarsening continuously which lead the stress value decrease. It can be seen from Fig. 4(d) that the stress-strain curves of 500–700 °C are obviously different which effect by dynamic precipitation on hardening. However, in the temperature stage of 700–900 °C, the static precipitation which affected the work-hardening process, and lead no differences in the shapes of the curves. The higher temperatures lead a lower stress value in. At the medium temperature zone (700–800 °C), the flow stress increases rapidly with the increase of the strain and then decreases gradually. Dynamic recrystallization occurs in some areas, which makes the dislocations arrangement into low-energy structures or disappear. However, at high deformation temperature range of (800–900 °C), both the particles coarsening and their partial dissolution release the grain boundary migration and then dynamic recrystallization occurs. Thus, the stress decreases and then reaches a stable value. Dynamic recovery is the most effective softening process which controls the follow stress level during hot deformation of the over aged copper alloy [21].

Compare with the stress-strain curves in Fig. 3, the stress values of the Cu-Ni-Co-Si-Cr alloy are higher than the Cu-Ni-Co-Si alloy under the same conditions which indicated that Cr strengthened the alloy. On the one hand, Cr addition refines the grains and improves the strength. Furthermore, Cr lead the precipitates improve and the precipitates pin the grain boundaries and dislocations which finally increased the true stress of the alloy [22].

3.2. Constitutive equation

The above flow stress was used to characterize the plastic deformation of the material. The constitutive equation can relate the flow stress

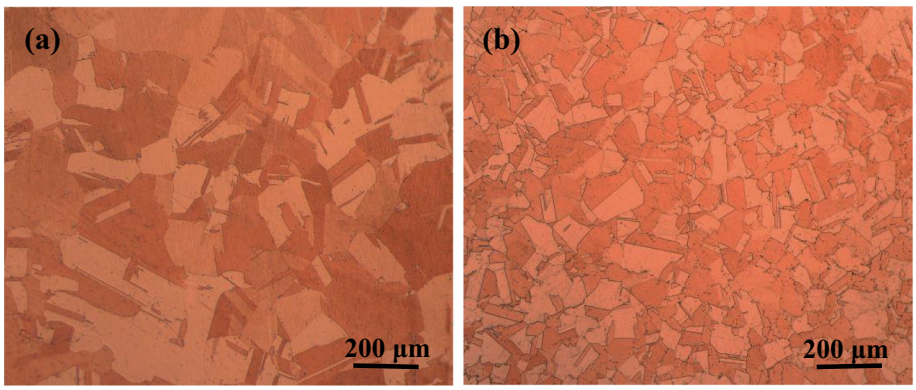

Fig. 2. The microstructure of (a) solid-solution Cu-Ni-Co-Si alloy; (b) solid-solution Cu-Ni-Co-Si-Cr alloy.

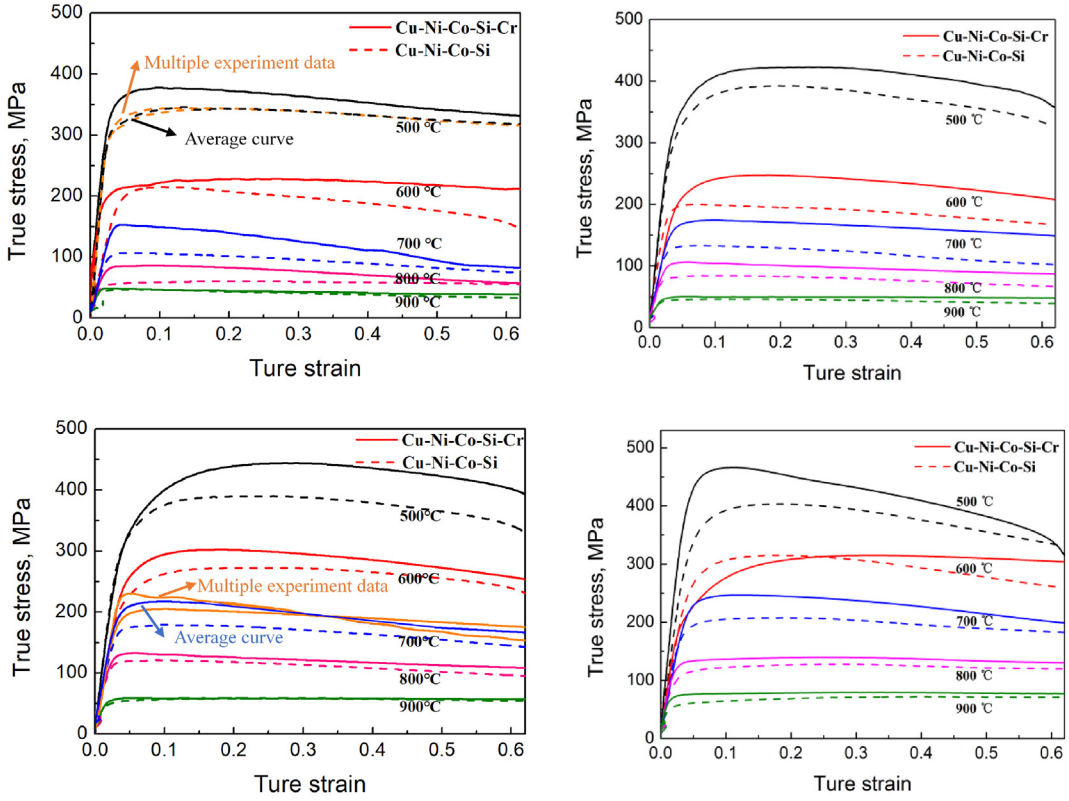

Fig. 3. True stress-true strain curves of the Cu-Ni-Co-Si and Cu-Ni-Co-Si-Cr alloys deformed at different temperatures and strain rates: (a) 0.001 s^{-1}; (b) 0.01 s^{-1}; (c) 0.1 s^{-1}; (d) 1 s^{-1}.

(σ), deformation temperature (T) and strain rate (ε), and describe the behavior of the flow stress at high temperatures, which can be expressed as follows:

$$\varepsilon = A_1\sigma^{n_1}\ \exp\left[-\frac{Q}{RT}\right] \alpha\sigma<0.8 \tag{1}$$

$$\varepsilon = A_2\ \exp(\beta\sigma)\ \exp\left[-\frac{Q}{RT}\right] \alpha\sigma>1.2 \tag{2}$$

$$\varepsilon = A[\ \sinh(\alpha\sigma)]^n\ \exp\left[-\frac{Q}{RT}\right] (\text{For all}) \tag{3}$$

Eq. (3) is used to represent the connection between the three variables proposed by Sellars [23]. Z is Zener-Hollomon parameter [24]; the effects of temperature and deformation rate on flow stress are defined according to the Zener-Hollomon [25–28].

$$Z = [\ \sinh(\alpha\sigma)]^{\mathrm{n}} = \varepsilon\ \exp\left[-\frac{Q}{RT}\right] \tag{4}$$

In equations of (1–4), A, A_1, A_2, α, β, n, and n_1 are the material constants, Q is the thermal activation energy (J/mol), R is the universal gas constant ($R = 8.31$ J/mol·K). By taking the logarithm of both sides of the Eqs. (1)–(3) were shown as follows:

$$\ln\varepsilon = n_1\ \ln\sigma + \ \ln A_1 - \frac{Q}{RT} \tag{5}$$

$$\ln\varepsilon = \beta\sigma + \ \ln A_2 - \frac{Q}{RT} \tag{6}$$

$$\ln\varepsilon = n\ \ln[\ \sinh(\alpha\sigma)] - \frac{Q}{RT} + \ \ln A \tag{7}$$

Here, n_1 and β are the average values of slopes in Fig. 4(a) and Fig. 4(b), which are expressed as the relationship between lnε and lnσ, and σ. Taking Cu-Ni-Co-Si alloy as an example, $n_1 = 12.569$ and $\beta = 0.113$, $\alpha = \beta/n_1 = 0.0089$. The n is an average of the slopes of lnε and ln [sinh$\alpha\sigma$] in Fig. 4(c), $n = 13.373$. Then the deformation activation energy (Q) is defined as:

$$Q = R\left[\frac{\partial\ \ln\varepsilon}{\partial\ \ln[\ \sin(\alpha\sigma)]}\right]_T\left[\frac{\partial\ \ln[\ \sinh(\alpha\sigma)]}{\partial(1/T)}\right] = RnS \tag{8}$$

Here, S is the slope of In[sinh$\alpha\sigma$] - 1000/T in Fig. 4(d), $S = 7.846$. By using S in Eq. (8), one can calculate an average activation energy of 569.8 kJ/mol. Fig. 4(e) shows a linear relationship between InZ and In [sinh$\alpha\sigma$]. The relationship is as follows:

$$\ln Z = \ \ln A + n\ \ln\ \sinh(\alpha\sigma) \tag{9}$$

ln$A$ is the intercept of Fig. 4(e), which can be obtained as $A = 63.38$. The constitutive equations for the Cu-Ni-Co-Si alloy can be expressed as follows:

$$\varepsilon = e^{63.38}[\ \sinh(0.009\sigma)]^{9.04}\ \exp\left(-\frac{569.8}{RT}\right) \tag{10}$$

According to the above methods, the constitutive equation for the Cu-Ni-Co-Si-Cr alloy was shown as follow:

$$\varepsilon = e^{75.35}[\ \sinh(0.005\sigma)]^{13.37}\ \exp\left(-\frac{639.5}{RT}\right) \tag{11}$$

The deformation activation energy of the Cu-Ni-Co-Si and Cu-Ni-Co-Si-Cr alloys is 569.8 kJ/mol and 639.5 kJ/mol, respectively. Fig. 8 shows TEM micrographs of the Cu-Ni-Co-Si and Cu-Ni-Co-Si-Cr alloys deformed at 800 °C and 0.001 s^{-1}. Obviously, with the Cr addition has a

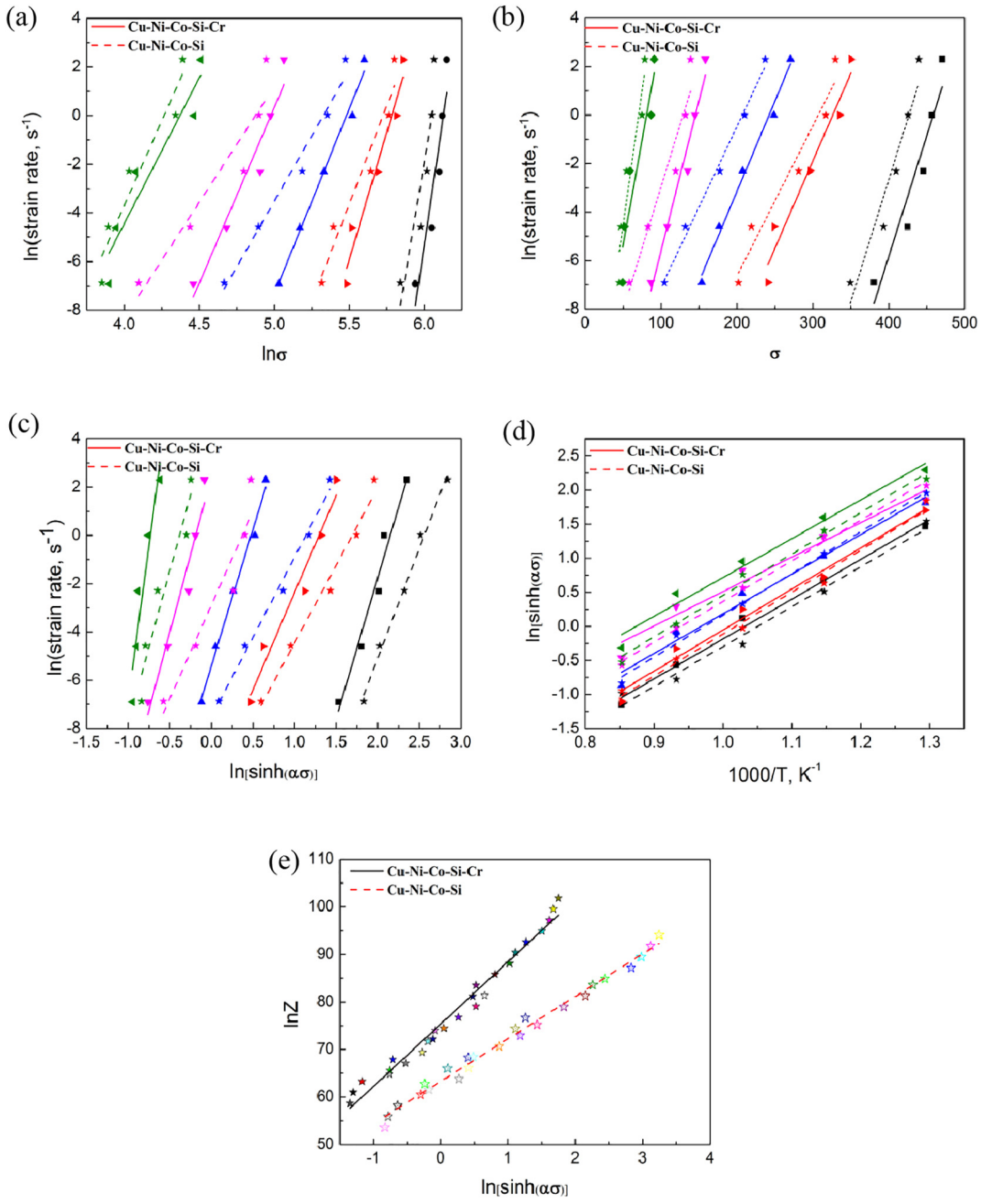

Fig. 4. Relations between: (a) ln $\dot{\varepsilon}$ - ln σ; (b) ln $\dot{\varepsilon}$ - σ; (c) ln $\dot{\varepsilon}$ - ln[sinh$\alpha\sigma$]; (d) ln[sinh$\alpha\sigma$] - 1000/T; (e) ln Z - ln[sinh$\alpha\sigma$].

significant impact on the precipitations [29]. With the Cr addition can increase more and finer precipitated phases in the matrix. The precipitated phase exists in the matrix and grain boundaries can inhibit the dislocation motion and difficult to move. In addition, the addition of Cr can effectively reduce the grain size and improve the microstructure more uniform. Due to the grain refinement, the dislocation movement is difficult and overcome the obstacle required more energy. Thus, it has much higher activation energy. In fact, activation energy is only one of the mathematical parameter for tested samples. Many processes are involved during hot working, each having its own Q value that means the activation energy has no clear meaning [10,30].

3.3. Microstructure evolution

Fig. 5(a) shows the microstructure of the Cu-Ni-Co-Si alloy deformed at 800 °C and 0.001 s^{-1}. It can be found that a large number of elongated bands appeared, which was related with the flow softening. The elongated bands were shown to spread from boundary to grain interior with the temperature increased and the strain rate decreased. Very fine recrystallized grains were observed at the grain boundaries, which is a typical characteristic of dynamic recrystallization [31]. The magnified view of the selected area is illustrated in Fig. 5(b), which clearly demonstrates the generation of fine dynamic recrystallized grains. Dynamic recrystallization nucleates preferentially at the grain boundaries, in which high distortion energy provides nucleation sites for dynamic recrystallization [32]. According to the investigation on hot deformation of Cu-Ni-Si-Cr-Mg alloy from L. Blaz et al. [10,11], and found that the nohomogeneous precipitation showed in the sheared areas was clearly observed with a high magnification. The reason is that the localized flow accelerated the precipitation coarsening in a sheared area and dynamically coarsened particles leaded the progressive local softening in the matrix. In terms of structure, it should be

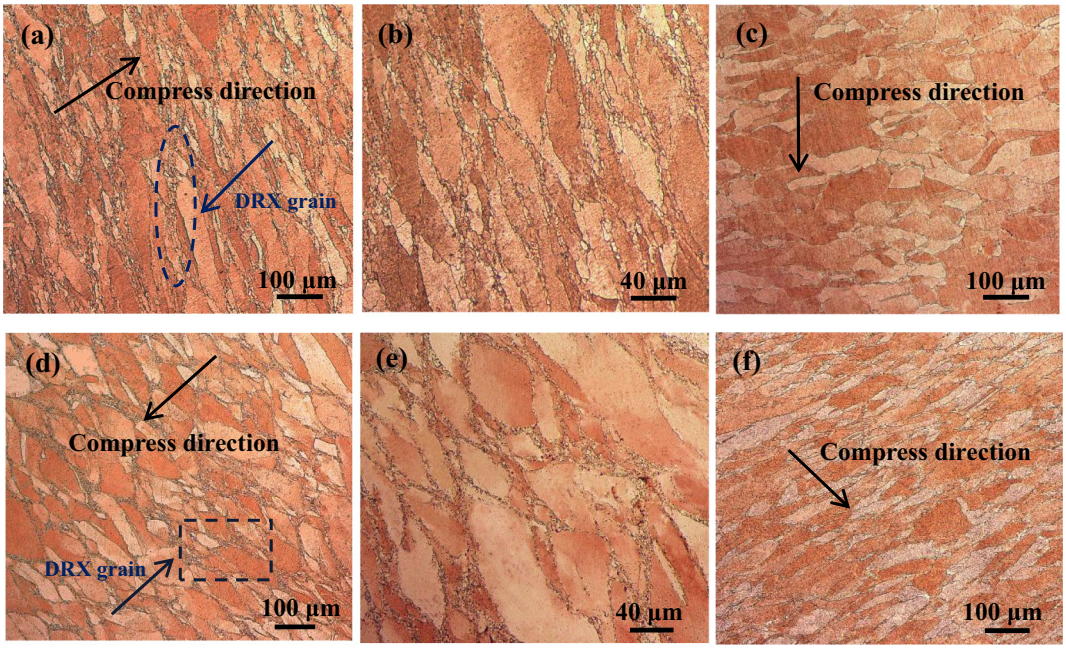

Fig. 5. The microstructure of the Cu-Ni-Co-Si and Cu-Ni-Co-Si-Cr alloys under different hot deformation conditions: (a) Cu-Ni-Co-Si alloy deformed at 800 °C and 0.001 s^{-1}, (b) magnification of DRX grains in (a), (c) Cu-Ni-Co-Si alloy deformed at 900 °C and 0.001 s^{-1}. (d) Cu-Ni-Co-Si-Cr alloy deformed at 800 °C and 0.001 s^{-1}, (e) magnification of DRX grains in (d), (f) Cu-Ni-Co-Si-Cr alloy deformed at 900 °C and 0.001 s^{-1}.

emphasized that the abnormal coarsening of dispersive particles at sheared area may take place in dynamic conditions only, i.e. during hot deformation of previously solution treated alloy. Moreover, shearing of the material finally lead cavity growth, and resulted in specimen fracture upon larger strain. Under these conditions, dynamic recrystallization rate of the alloy is high, which can effectively eliminate the peak stress during the work hardening process. Similarly, the same recrystallized grains were found in the Cu-Ni-Co-Si-Cr alloy, as shown in Fig. 5(d) and Fig. 5(e). Dynamically recrystallized grains are also formed preferentially at grain boundaries. Compared with the size of the newly generated recrystallized grains, it can be seen that the Cr addition inhibits the alloy recrystallization. At higher temperature, the fine grains were gradually replaced by the coarse structure in the matrix and grew continuously. Fig. 5(c) and Fig. 5(f) show the microstructure of the Cu-Ni-Co-Si and Cu-Ni-Co-Si-Cr alloys deformed at 900 °C and 0.001 s^{-1}. At low temperature, the boundary migration is difficult. However, the grain boundary migration is easy as the temperature increases. Close to the solvus temperature during deformation, the fine particles dissolved and released, which improve the grain boundary migrate easy. [33,34].

3.4. EBSD

Fig. 6(a) and Fig. 6(b) are the EBSD micrographs of the Cu-Ni-Co-Si and Cu-Ni-Co-Si-Cr alloys deformed at 800 °C and 0.001 s^{-1}, respectively. The inverse pole figure (IPF) and grain orientation maps show that the DRX grains begin to nucleate at grain boundaries. Compared with the Cu-Ni-Co-Si alloy deformed at 900 °C and 0.001 s^{-1} was shown in Fig. 6(c), small DRX grains grow further at high temperatures. The reason is that the higher temperatures provide higher mobility to the grain boundaries for nucleation and growth of the DRX grains. Fig. 6(d) shows the misorientation angle values of the Cu-Ni-Co-Si alloy at different temperatures. It can be observed that the misorientation angle of 14.19° at 800 °C is significantly smaller than the misorientation angle of 24° with the recrystallization is completed at 900 °C. While the grain misorientation value of both sides of the grain boundary is small, the migration velocity of the grain boundary is smaller. Therefore, the migration velocity of grain boundary during recrystallization is smaller than that at 900 °C with the recrystallization was completed [35,36]. Fig. 6 also shows the pole figures of the samples deformed at different temperatures. At 800 °C, the Goss {011}⟨100⟩ texture and cubic {001}⟨100⟩ texture appeared in Cu-Ni-Co-Si (Fig. 6a), while the texture of Cu-Ni-Co-Si-Cr was copper {112}⟨111⟩ texture, the Goss {011}⟨100⟩ texture and cubic {001}⟨100⟩ texture (Fig. 6b). Generally, the Goss texture is a texture widely formed during dynamic recrystallization. With the increase of temperature, dynamic recrystallization particles grow and coarsen further, and the Goss texture in Cu-Ni-Co-Si was replaced by the brass {011}⟨112⟩ texture (Fig. 6c) [37].

3.5. Microstructure of solution treatment samples

Fig. 7 shows the crystal structure of some precipitates in the alloy. The lattice parameters of the Ni_2Si and Co_2Si phases are quite similar, and they have the same structure. However, Ni_2Si has orthorhombic structure a = 0.709 nm, b = 0.490 nm and c = 0.372 nm, Pbnm (62) [38], while the lattice parameters of Co_2Si are a = 0.710 nm, b = 0.491 nm, and c = 0.378 nm [39].

Fig. 8 shows the TEM micrographs of the Cu-Ni-Co-Si and Cu-Ni-Co-Si-Cr alloys deformed at 800 °C and 0.001 s^{-1}. A large number of nano-scaled precipitates and the presence of the dislocations can be clearly observed. Precipitates exist in the matrix and hinder the movement of dislocations. Compared with the size of the precipitates in the Cu-Ni-Co-Si and Cu-Ni-Co-Si-Cr alloys, it was obviously observed that the size of the precipitates of the alloy containing Cr is relatively small. It can be concluded that with the addition of Cr can lead the size of the precipitate reduce and the number of precipitates increase. The precipitates are distributed uniformly in the matrix. Furthermore, the strengthening effect of the precipitation is more obviously obtained and much more the strength while the precipitated phase is fine.

Fig. 9 shows the TEM (HRTEM) micrographs and the selected-area diffraction patterns (SADP) of the Cu-Ni-Co-Si alloy deformed at 800 °C and 0.001 s^{-1}. The selected area electron diffraction pattern shows the precipitates with two different shapes in Fig. 9(a), which are rod-shaped and spherical-shaped, respectively [40]. In the dynamic

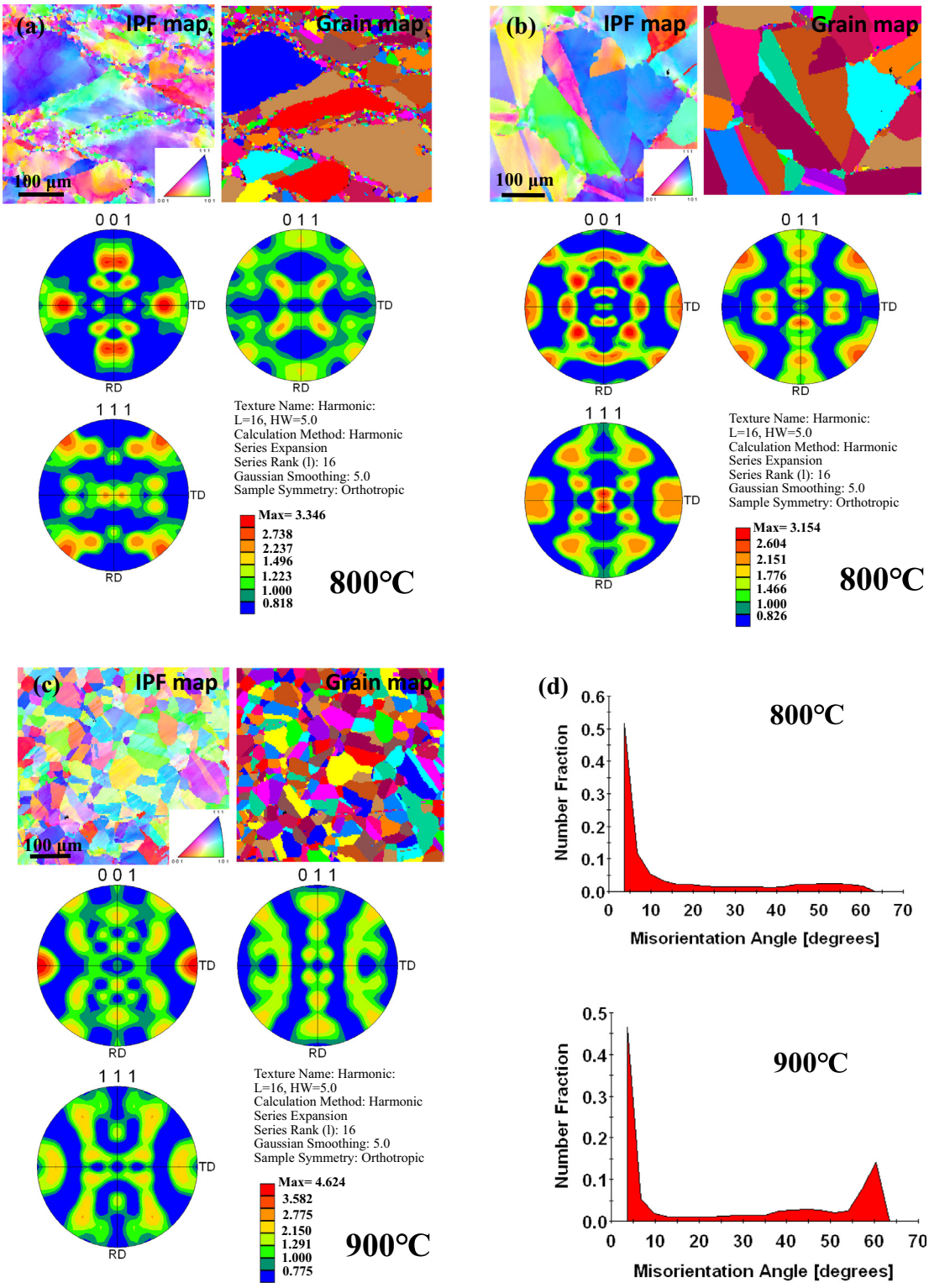

Fig. 6. EBSD micrographs and Pole figures at different alloy and temperatures. (a) Cu-Ni-Co-Si alloy deformed at 800 °C and 0.001 s^{-1}, (b) Cu-Ni-Co-Si-Cr alloy deformed at 800 °C and 0.001 s^{-1}, (c) Cu-Ni-Co-Si alloy deformed at 900 °C and 0.001 s^{-1}, (d) misorientation angle of Cu-Ni-Co-Si alloy at 800 °C and 900 °C.

precipitation process, many researches have shown that the coarse particles with rodlike and spherical in shape at large strain, and the needle-like precipitates appeared at some grain boundaries at low strain [10,41]. Fig. 9(b) and Fig. 9(c) show the dark field micrographs and the corresponding SADP patterns along [001] Cu, respectively, which verifies that the precipitate is δ-Ni_2Si. Fig. 9(d) shows the X-ray diffraction (XRD) pattern of the rod-shaped precipitate. It demonstrates that there are many Co atoms in the precipitate, and the ratio of (Ni, Co): Si is about 2:1. Due to the similar atomic radii of Ni and Co, a part of Ni atoms in the Ni_2Si phase can be replaced by Co atoms, forming $(Ni, Co)_2Si$. Therefore, it is believed that there is no single Ni_2Si, but $(Ni, Co)_2Si$ precipitated phase. Fig. 9(e) shows the HRETEM micrograph and the

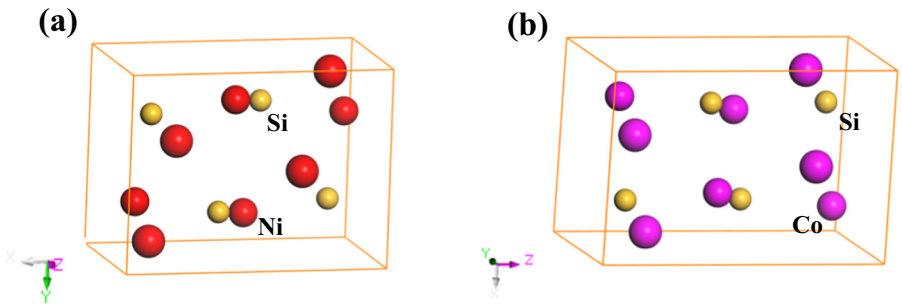

Fig. 7. Schematics of the precipitates crystal structure: (a)δ-Ni_2Si; (b) Co_2Si.

corresponding inverse fast Fourier transform (FFT) patterns of the (Ni, Co)$_2$Si phase. According to the inverse FFT pattern, the lattice size of the precipitate lattice was measured to be consistent with the (Ni, Co)$_2$Si precipitate. Moreover, Fig. 9(f) shows the size of the larger precipitate is 365 nm, and the SADP image shows that the precipitate is coarse (Ni, Co)$_2$Si.

Fig. 10 shows the TEM (HRTEM) micrographs and the SADPS of the Cu-Ni-Co-Si-Cr alloy deformed at 800 °C and 0.001 s^{-1}. In Fig. 10(a), it can be found that a large number of dislocations are entangled and formed dislocation cells, due to the pinning effect of the precipitates, which hinder the dislocation movement. Fig. 10(b) shows the dark-field micrograph of Fig. 10(a). It can be clearly seen that the distribution of the precipitates has higher density and the size is smaller than the Cu-Ni-Co-Si alloy. Additionally, it also indicates that addition of Cr promotes precipitation and refines grains. Fig. 10(c) and Fig. 10(d) show the SADP along [001] Cu and the HRETEM micrograph, respectively. Obviously, the size of the (Ni, Co)$_2$Si is much smaller than that without Cr. Fig. 10 (e) shows a precipitate with large square particles imbedded in the matrix, which can be concluded from the SADP that it is Co_2Si. Fig. 10 (f) shows the coarsened rod-shaped (Ni, Co)$_2$Si.

The precipitates play a significant role in strengthening the matrix. For instance, the precipitated (Ni, Co)$_2$Si phase are observed along in the dislocation and grain boundaries, thus hindering the movement and delaying the process of dynamic recrystallization. Moreover, the formation of Co_2Si can inhibit grain growth and improve softening resistance. Noticeably, according to our work, it is shown that the addition of Cr can effectively promote the generation of the precipitates and reduce the grain size resulting in the strengthening of the alloy [42]. This also explains why the strength of the Cu-Ni-Co-Si-Cr alloy is higher than the Cu-Ni-Co-Si alloy.

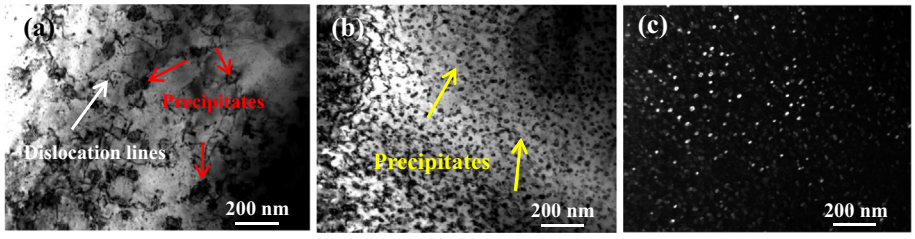

Fig. 8. TEM micrographs of samples deformed at 800 °C and 0.001 s^{-1}: (a) Cu-Ni-Co-Si; (b) Cu-Ni-Co-Si-Cr; (c) dark-field micrograph of (b).

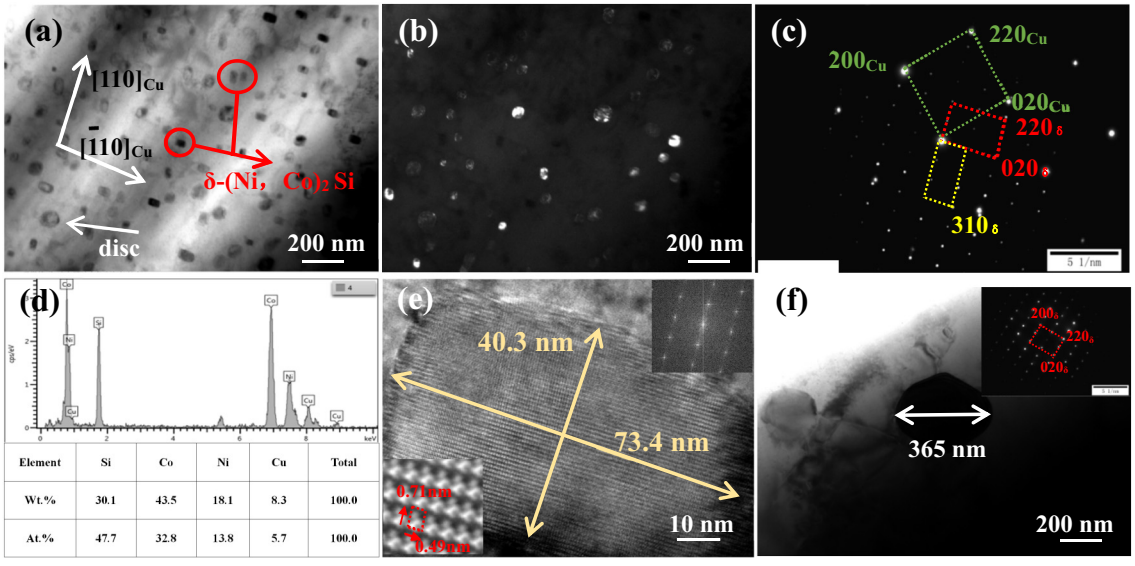

Fig. 9. TEM micrographs and SADPs of the Cu-Ni-Co-Si alloy deformed at 800 °C and 0.001 s^{-1}; (a) bright-field micrograph; (b) dark-field micrograph of (a); (c) beam direction of SADP along [001]Cu; (d) XRD analysis of (a); (e) HRTEM of the δ-(Ni,Co)$_2$Si; (f) SADP and TEM of the large precipitation phase.

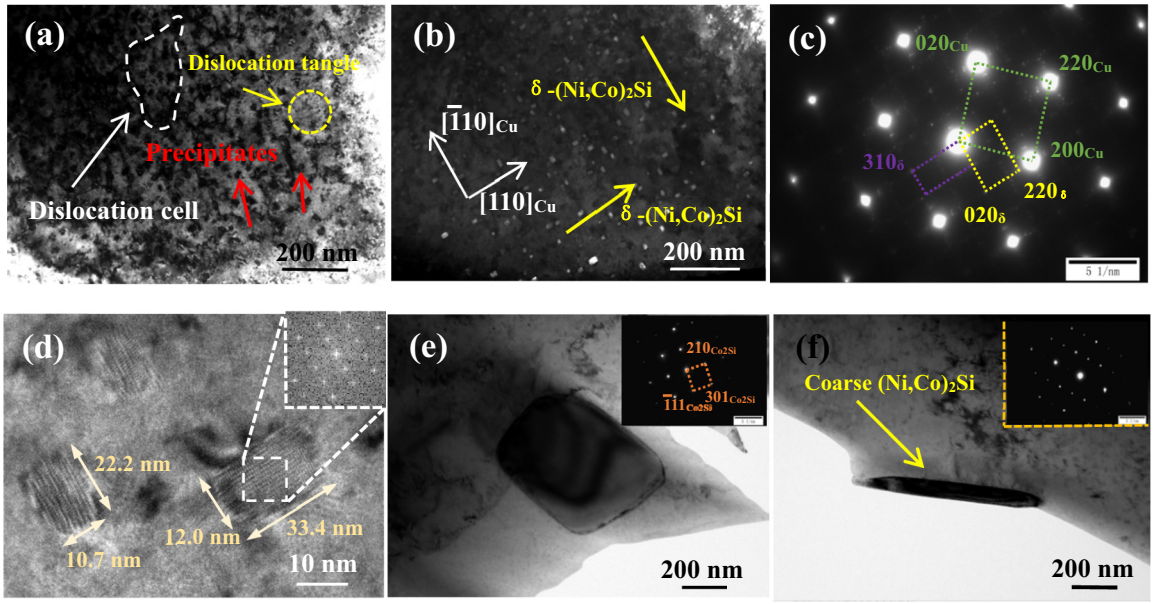

Fig. 10. TEM micrographs and SADPS of the Cu-Ni-Co-Si-Cr alloy deformed at 800 °C and 0.001 s^{-1}; (a) bright-field micrograph; (b) dark-field micrograph of (a); (c) beam direction of SADP along [001]Cu; (d) HRTEM of the δ-(Ni, Co)$_2$Si; (e) bright-field micrograph and SADP of Co_2Si; (f) bright-field micrograph and SADP of δ-(Ni, Co)$_2$Si.

Fig. 11(a) and Fig. 11(b) show the distribution of the precipitates in the Cu-Ni-Co-Si alloy. Disorderly dislocations and the precipitates interact with each other as show in Fig. 11(a). As shown in Fig. 11(b), the precipitates pinned sub-grain boundaries, which effectively hinder the migration of sub-grain boundaries. Fig. 11(d) shows the deformation zone of the alloy during thermal deformation, and the deformation zone has different degrees of dislocation density, and the dislocation density of the cell boundary is much higher than that inside the cells. At this time, the deformation zone will transform into cellular substructure, which is also called "quasi-sub crystalline structure" [19]. Fig. 11(e) shows the dark field micrograph of Fig. 11(d), where the nanoscale precipitation is distributed on the dislocations, grain boundaries, and the matrix.

Fig. 11(f) and Fig. 11(g) show the precipitates at the grain boundary, respectively. Compared with the precipitates which inside the grain, it can be seen that the nonhomogeneous coarse (Ni, Co)$_2$Si particles show at the grain boundary. Flow localization in solution-treated specimens, which resulted in dynamic coarsening of precipitates at grain boundaries at low strain, was expanded into grain interiors at larger strains. Moreover, the process becomes self-induced as dynamic coarsening softens the matrix and allows the flow localization to continue.

4. Discussion

4.1. Effect of Cr on the precipitation phase

According to the experimental data and the selected area diffraction patterns analysis, the Cu-Ni-Co-Si alloy will produce a series of precipitates after thermal compression. Compared with the aging precipitation at 500 °C of the Cu-Ni-Co-Si alloy studied by Li [43], the aging precipitation at 450 °C of the Cu-Ni-Si alloy reported by Lei [44] and the Cu-Ni-Si-Cr alloy aging precipitation studied by Cheng [18], similar research results were obtained during the heat treatment process.

The (Ni, Co)$_2$Si, and Co_2Si phases precipitated at 800 °C and 0.001 s^{-1} in our work. Moreover, with the addition of Cr element, more precipitates were produced. The precipitates exist at grain boundaries or dislocations, which hinderer their movement, and finally improved the alloy strength. Furthermore, with the addition of Cr, the alloy structure was refined.

4.2. Effect of Cr on the microstructure of Cu-Ni-Co-Si alloy

The addition of Cr element can increase the flow stress of the alloy due to reduced grain size of the alloy. Compared with the structure of the Cu-Ni-Co-Si and Cu-Ni-Co-Si-Cr alloys after solid solution in Fig. 2, the effect of the grain size refinement is obviously observed.

4.3. Precipitation strengthening mechanism

The strength improvement of the alloy includes the following aspects such as precipitation strengthening, grain refinement strengthening, work hardening, and solid solution strengthening. Precipitation strengthening is the dominant role of alloy strength, and the very fine and coherent precipitation are more beneficial the strengthening of the alloy. In this experiment, the addition of Cr can obtain more precipitates, and the precipitates pined at the grain boundaries and dislocations, which can hinderer the movement of dislocations and grain boundaries, and finally increased the strength. Meanwhile, the dynamic precipitation in the hot deformation is also another factor affect the strength of the alloy. In the medium temperature zone (500–700 °C), dynamic precipitation increased the strength of the alloy most obviously. With the increased of temperatures, the precipitations coarsen, and the strength and hardness of the material decreased. In addition, the precipitates exist in the grain boundary which can lead the strength and hardness of the alloy much higher than precipitates in the grain interiors. Thus, the location for the precipitates can also affect the strength and hardness of the alloy.

4.4. Grain refinement strengthening mechanism

The recrystallized grains are formed in the thermal deformation process, and the boundary of the substructure can hinderer the movement of the dislocation and improves the strength. The effect of the cell subgrain size on the strength can be expressed by Hall-Petch [45] equation:

$$\Delta\sigma_{grain\ refinement} = \frac{K}{\sqrt{d_{grain}}} \tag{12}$$

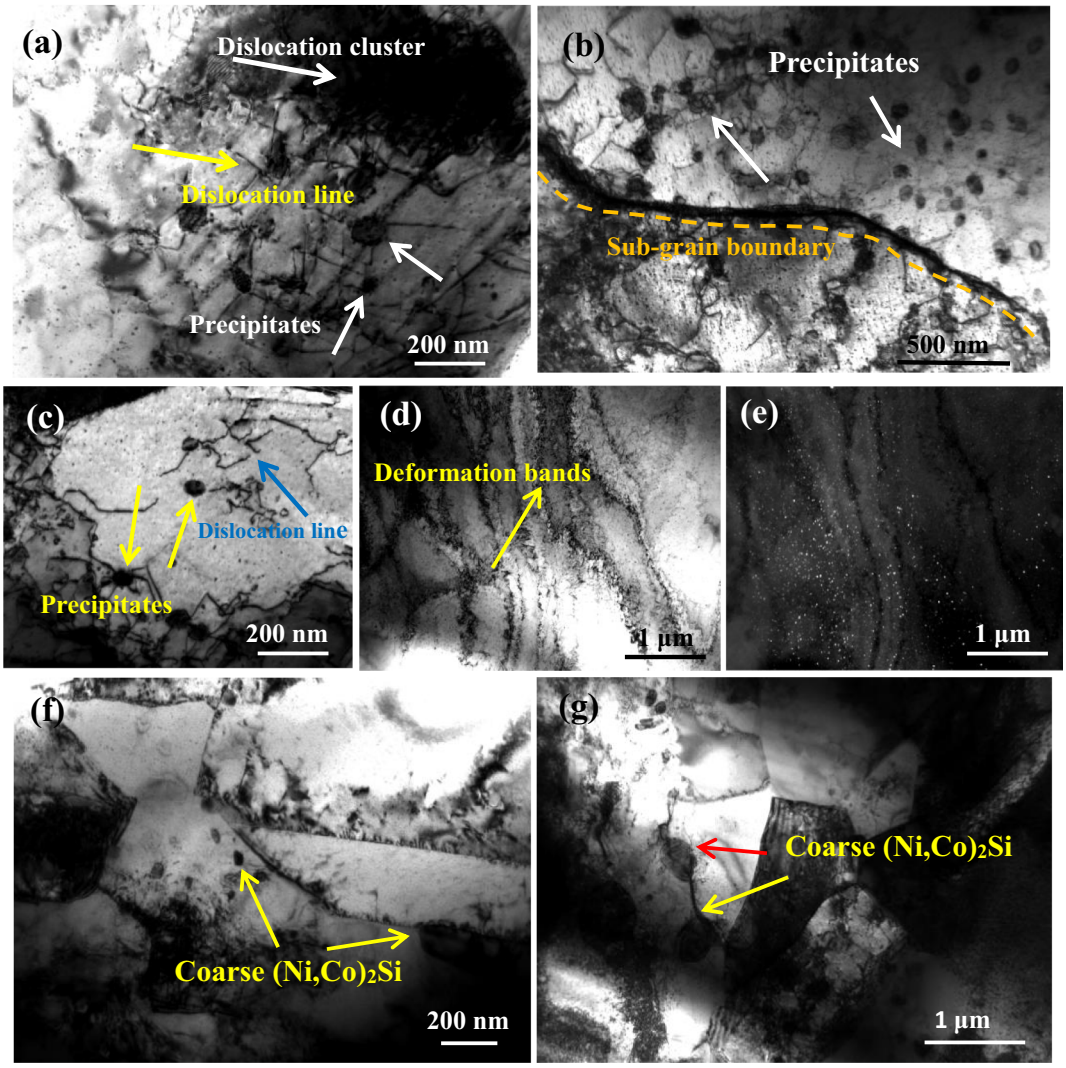

Fig. 11. (a) and (b) show the TEM micrographs of Cu-Ni-Co-Si alloy at the thermal deformation temperature of 800 °C and 0.001 s^{-1}. (c), (d), (e), (f), (g) show the TEM micrographs of Cu-Ni-Co-Si-Cr alloy at the thermal deformation temperature of 800 °C and 0.001 s^{-1}.

Here, K is a constant for copper alloys, d_{grain} is the average diameter of grains (the value was measured from TEM micrographs). The obtained grain refinement strength is listed in Table 2.

The flow stress and strength of the alloy were increased by grain refinement and the precipitation. The precipitation increases the activation energy and improves the high temperature stability of the alloy. Moreover, the addition of Cr makes the structure more uniform in the process of thermal deformation. Consequently, the Cu-Ni-Co-Si-Cr alloy has better stability at high temperatures.

5. Conclusions

Hot deformation of the Cu-Ni-Co-Si and Cu-Ni-Co-Si-Cr alloys was conducted at the deformation temperature ranging from 500 °C to 900 °C and strain rate ranging from 0.001 s^{-1} to 10 s^{-1}. The following conclusions were obtained:

(1) Flow stress decreases with the deformation temperature and increases with the strain rate. Dynamic precipitation has the most obviously effect at medium temperature (500–700 °C). The occurrence of dynamic precipitation increases the value of flow stress.

(2) The addition of Cr refines the grain, improves activation energy of the alloy, which are 569.8 kJ/mol and 639.5 kJ/mol, respectively. The constitutive equations of the Cu-Ni-Co-Si and Cu-Ni-Co-Si-Cr alloy are: $\varepsilon = e^{63.38}[\sinh(0.009\sigma)]^{9.04}\exp(-\frac{569.8}{RT})$ and $\varepsilon = e^{75.35}[\sinh(0.005\sigma)]^{13.37}\exp(-\frac{639.5}{RT})$, respectively.

(3) The misorientation angle increased with the recrystallization is completed according to the EBSD analysis. The texture of Cu-Ni-Co-Si alloy at 800 °C is the Goss {011}⟨100⟩ texture and {001}⟨100⟩ cubic texture, and the Goss texture at 900 °C is replaced by the brass {011}⟨112⟩ texture.

(4) The $(Ni, Co)_2Si$ and Co_2Si were obtained during the thermal compression process, which hinderer the dislocations and grain boundaries movement, and improved the strength and hardness

Table 2
The values of the grain refinement strengthening.

Alloy	K/MPa$\sqrt{M}$	d/μm	$\Delta\sigma_{GS}$/MPa
Cu-Ni-Co-Si	0.14	3.2	78.3
Cu-Ni-Co-Si-Cr	0.14	1.6	110.7

of the alloy.

(5) With the addition of Cr, the size of the precipitates reduced while the number of precipitates increased, which improved the alloy properties. Precipitation strengthening and Grain refinement are the main strengthening mechanisms.

CRediT authorship contribution statement

Yijie Ban: Investigation, Writing - original draft. **Yi Zhang:** Writing - review & editing. **Yanlin Jia:** Formal analysis. **Baohong Tian:** Methodology. **Alex A. Volinsky:** Writing - review & editing. **Xiaohui Zhang:** Investigation. **Qifei Zhang:** Investigation. **Yongfeng Geng:** Writing - review & editing. **Yong Liu:** Formal analysis. **Xu Li:** Investigation.

Acknowledgments

This work was supported by the Open Cooperation Project of Science and Technology of the Henan Province (182106000018), the Henan University Scientific and Technological Innovation Talent Support Program (18HASTIT024), the National Natural Science Foundation of China (U1704143) and the National Natural Science Foundation of China (U1502274).

References

[1] Q.Y. Dong, L.N. Shen, F. Cao, Y.L. Jia, K.J. Liao, M.P. Wang, Effect of thermomechanical processing on the microstructure and properties of a Cu-Fe-P alloy, J. Mater. Eng. Perform. 24 (2015) 1531–1539.
[2] Q. Lei, Z. Li, J. Wang, J.M. Xie, X. Chen, S. Li, Y. Gao, L. Li, Hot working behavior of a super high strength Cu-Ni-Si alloy, Mater. Des. 51 (2013) 1104–1109.
[3] A.Y. Khereddine, F.H. Larbi, M. Kawasaki, T. Baudin, D. Bradai, T.G. Langdon, An examination of microstructural evolution in a Cu-Ni-Si alloy processed by HPT and ECAP, Mater. Sci. Eng. A 576 (2013) 149–155.
[4] H. Tsubakino, R. Nozato, A. Yamamoto, Precipitation sequence for simultaneous continuous and discontinuous modes in Cu-Be binary alloys, Mater. Sci. Technol. 9 (1993) 288–294.
[5] Y. Zhang, B.H. Tian, A.A. Volinsky, X.H. Chen, H.L. Sun, Z. Chai, P. Liu, Y. Liu, Dynamic recrystallization model of the Cu-Cr-Zr-Ag alloy under hot deformation, J. Mater. Res. 31 (2016) 1275–1285.
[6] S. Satoshi, T. Takasugi, Fabrication of high-strength and high conductivity Cu-Ti alloy wire by aging in a hydrogen atmosphere, J. Alloy. Compd. 580 (2013) S397–S400.
[7] L.S. Silva, J.S. Souza, R.A.G. Silva, Effects of Ag addition on phase transitions, microstructures and solder/copper interfaces of $Sn_{99.1-x}Cu_{0.9}Ag_x$ alloys, J. Therm. Anal. Calorim. 136 (6) (2019) 2205–2210.
[8] S.A. Lockyer, F.W. Noble, Precipitate structure in a Cu-Ni-Si alloy, 24 Mater. Sci 29 (1) (1994) 218–226.
[9] X.J. Liu, S.L. Xiang, S.Y. Yang, R.P. Shi, C.P. Wang, Experimental investigation of phase equilibria in the Cu-Ni-Si ternary system, J. Alloys Compd. 578 (2013) 439–447.
[10] J. Li, G.J. Huang, X.J. Mi, L.J. Peng, H.F. Xie, Y.L. Kang, Effect of Ni/Si mass ratio and thermomechanical treatment on the microstructure and properties of Cu-Ni-Si alloys [J], Materials 12 (2019) 2076.
[11] L. Blaz, E. Evangelista, M. Niewczas, Precipitation effects during hot deformation of a copper alloy [J], Metallurgical & Materials Transactions A 25 (2) (1994) 257–266.
[12] M. Niewczas, E. Evangelista, L. Blaz, Strain localization during a hot compression test of Cu-Ni-Cr-Si-Mg alloy[J], Scr. Metall. Mater. 27 (12) (1992) 1735–1740.
[13] Q.S. Wang, G.L. Xie, X.J. Mi, B.Q. Xiong, X.P. Xiao, The precipitation and strengthening mechanism of Cu-Ni-Si-Co alloy, Mater. Sci. Forum (2013) 294–298.
[14] J.Z. Huang, Z. Xiao, J. Dai, Z. Li, H. Jiang, W. Wang, X. Zhang, Microstructure and properties of a novel Cu-Ni-Co-Si-Mg alloy with super-high strength and conductivity, Mater. Sci. Eng. A 744 (2019) 754–763.
[15] Z. Zhao, Y. Zhang, H.B. Tian, Y.L. Jia, Y. Liu, K.X. Song, A.A. Volinsky, Co effects on Cu-Ni-Si alloys microstructure and physical properties[J], J. Alloys Compd. 797 (2019) 1327–1337.
[16] Y.K. Wu, Y. Li, J.Y. Lu, S. Tan, F. Jiang, J. Sun, Correlations between microstructures and properties of Cu-Ni-Si-Cr alloy [J], Mater. Sci. Eng. A 731 (2018) 403–412.
[17] W. Wang, H. Kang, Z. Chen, Z. Chen, C. Zou, R. Li, G.M. Yin, T.M. Wang, Effects of Cr and Zr additions on microstructure and properties of Cu-Ni-Si alloys, Mater. Sci. Eng. A 673 (2016) 378–390.
[18] J.Y. Cheng, B.B. Tang, F.X. Yu, B. Shen, Evaluation of nanoscaled precipitates in a Cu–Ni–Si–Cr alloy during aging, J. Alloy. Compd. 614 (2014) 189–195.
[19] Z.L. Zhao, Z. Xiao, Z. Li, W.T. Qiu, H.Y. Jing, Q. Lei, Z. Liu, Y.B. Jiang, S.J. Zhang, Microstructure and properties of a Cu–Ni–Si–Co–Cr alloy with high strength and high conductivity[J], Mater. Sci. Eng. A 759 (2019) 396–403.
[20] V. Patel, W.Y. Li, Q. Wen, Y. Su, N. Li, Stationary Shoulder Friction Stir Processing: A Low Heat Input Grain Refinement Technique for Magnesium Alloy[M]//Friction Stir Welding and Processing X, Springer, Cham, 2019 209–215.
[21] A.A. Hameda, L. Blaz, Microstructure of hot-deformed Cu-3.45 wt.% Ti alloy[J], 254 (1–2) (1998) 83–89.
[22] N.T. Kareva, I.L. Yakovleva, O.V. Samoilova, On the precipitation strengthening of Cu–2.6Ni–0.6Si–0.6Cr bronzes[J], Phys. Met. Metallogr. 118 (2017) 795–801.
[23] C.M. Sellars, W.J. McTegart, On the mechanism of hot deformation, Acta Metall. 14 (1966) 1136–1138.
[24] C. Zener, J.H. Hollomon, Effect of strain-rate upon the plastic flow of steel, J. Appl. Phys. 15 (1994) 22–27.
[25] F.A. Slooff, J. Zhou, J. Duszczyk, et al., Constitutive analysis of wrought magnesium alloy Mg–Al4–Zn1[J], Scr. Mater. 57 (2007) 759–762.
[26] B.J. Wang, Y. Zhang, B.H. Tian, et al., Effects of Ce addition on the Cu-Mg-Fe alloy hot deformation behavior [J], Vacuum 155 (2018) 594–603.
[27] S.F. Medina, C.A. Hernandez, General expression of the Zener-Hollomon parameter as a function of the chemical composition of low alloy and microalloyed steels[J], Acta Mater. 44 (1) (1996) 137–148.
[28] Z. Xu, Y. Liu, H. Hu, et al., Thermo-viscoplastic behavior and constitutive modeling of pure copper under high-strain-rate shear condition [J], Mech. Mater. 129 (2019) 306–319.
[29] S. Saadatkia, H. Mirzadeh, J.M. Cabrera, Hot deformation behavior, dynamic recrystallization, and physically-based constitutive modeling of plain carbon steels [J], Mater. Sci. Eng. A 636 (2015) 196–202.
[30] B. Pourbahari, H. Mirzadeh, M. Emamy, The effects of grain refinement and rare earth intermetallics on mechanical properties of as-cast and wrought magnesium alloys[J], J. Mater. Eng. Perform. 27 (2018) 1327–1333.
[31] N.N. Guo, L. Wang, L.S. Luo, X.Z. Li, R.R. Chen, Y.Q. Su, J.J. Guo, H.Z. Fu, Hot deformation characteristics and dynamic recrystallization of the Mo-Nb-Hf-Zr-Ti refractory high-entropy alloy [J], Mater. Sci. Eng. A 651 (2016) 698–707.
[32] H. Jiang, J. Dong, M. Zhang, Z.H. Zhao, A study on the effect of strain rate on the dynamic recrystallization mechanism of alloy 617B [J], Metall. Mater. Trans. A 47 (2016) 5071–5087.
[33] T.W. Wong, A. Hadadzadeh, M.S. Wells, High temperature deformation behavior of extruded AZ31B magnesium alloy [J], J. Mater. Process. Technol. 251 (2018) 360–368.
[34] L. Blaz, E. Evangelista, Strain rate sensitivity of hot deformed Al and AlMgSi alloy[J], Mater. Sci. Eng. A 207 (2) (1996) 195–201.
[35] R. Sonkusare, A. Swain, M.R. Rahul, S. Samal, N.P. Gurao, K. Biswas, S.S. Singh, N. Nayan, Establishing processing-microstructure-property paradigm in complex concentrated equiatomic Co-Cu-Fe-Mn-Ni alloy [J], Mater. Sci. Eng. A 759 (2019) 415–429.
[36] K. Sahithya, I. Balasundar, P. Pant, T. Raghu, H.K. Nandi, V. Singh, P. Ghosal, M. Ramakrishna, Deformation behaviour of an as-cast nickel base superalloy during primary hot working above and below the gamma prime solvus [J], Mater. Sci. Eng. A 754 (2019) 521–534.
[37] Q. Lei, Z. Li, W.P. Hu, Y. Liu, C.L. Meng, B. Derby, W. Zhang, Microstructure evolution and hardness of an ultra-high strength Cu-Ni-Si alloy during thermo-mechanical processing[J], J. Mater. Eng. Perform. 25 (2016) 2615–2625.
[38] K. Toman, The structure of Ni_2Si, Acta Crystallogr. 5 (3) (1952) 329–331.
[39] S. Geller, V.M. Wolontis, The crystal structure of Co_2Si, Acta Crystallogr. 8 (2) (1955) 83–87.
[40] J. Yi, Y.L. Jia, Y.Y. Zhao, Z. Xiao, K.J. He, Q. Wang, M.P. Wang, Z. Zhou, Precipitation behavior of Cu-3.0 Ni-0.72 Si alloy[J], Acta Mater. 166 (2019) 261–270.
[41] Y.L. Jia, M.P. Wang, C. Chen, Q.Y. Dong, S. Wang, Z. Li, Orientation and diffraction patterns of d-Ni2Si precipitates in Cu-Ni-Si alloy, J. Alloys Compd. 557 (25) (2013) 147–151.
[42] A.P. Zhilyaev, I. Shakhova, A. Morozova, A. Belyakov, R. Kaibyshev, Grain refinement kinetics and strengthening mechanisms in Cu–0.3Cr–0.5Zr alloy subjected to intense plastic deformation [J], Mater. Sci. Eng. A 654 (2016) 131–142.
[43] J. Li, G. Huang, X. Mi, et al., Relationship between the microstructure and properties of a peak aged Cu–Ni–Co–Si alloy [J], Mater. Sci. Technol. 35 (5) (2019) 606–614.
[44] Q. Lei, L. Zhou, G. Yang, P. Xi, B. Derby, Microstructure and mechanical properties of a high strength Cu-Ni-Si alloy treated by combined aging processes [J], J. Alloys Compd. 695 (2017) 2413–2423.
[45] Z.C. Cordero, B.E. Knight, C.A. Schuh, Six decades of the Hall-Petch effect-a survey of grain-size strengthening studies on pure metals [J], Int. Mater. Rev. 61 (8) (2016) 495–512.